ASIPP

A+M Data Application in EAST Tokamak Edge Simulations of Impurity Seeding Plasma

Xiaoju Liu, Guozhong Deng, Shaochen Liu, Ling Zhang, Juang Huang, Xiang Gao and EAST Team

Institute of Plasma Physics, Chinese Academy of Sciences, PO Box 1126, Hefei 230031, China, Email:julie1982@ipp.ac.cn

1. Introduction

➢ **Controlling the excessive heat load to divertor targets is a critical issue for ITER and CFETR**—— to seed impurity with relatively high radiation loss rate, like N, Ne, Ar.

➢**Modeling is meaningful and necessary**—— to understand the radiative characters and distribution of different candicate radiators, to optimize the choice and puffing rate and to study the possible effect of impurity seeding on core performance.

➢**Atomic and Molecular (A+M) is crucial in detailed modeling**——to determine the interaction of the plasma constituents, and eventually to affect the power dispersal and momentum losses in plasma.

2. Simulation parameters

➢ **SOLPS5.0[1] = a 2D fluid code B2.5 + the 3D Monte-Carlo neutral code Eirene** —— good 2D code to describe SOL and divertor plasma and well applied in many fusion devices such as AUG, JET, DIII-D and ITER.

2.1. Computational grid and inputs

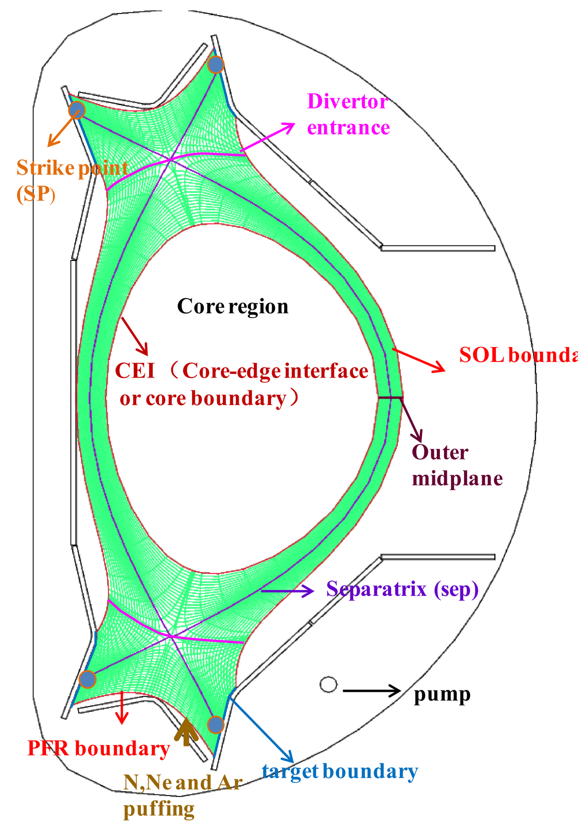

Fig. 1. Computational mesh for the SOLPS simulations.

➢**Modeling setups and assumptions**

✓CEI-core edge interface (core boundary)

• P_{CEI}=P_{in}-$P_{rad,core}$=1.6MW, P_{in}=2MW, 0.4MW (~20%) radative loss in core region not accounted in the simulations , equipartition between electron and ion.

• $n_{e,sep}$ =1.0×$10^{19}m^{-3}$at separatrix of outer midplane by feedback control through D_2 puff from SOL boundary.

• Radial diffusion coefficients D=0.3, $\chi_i = \chi_e$ =1.0. usually determined by fitting the upstream density and temperature profiles measured by RP and edge TS.

✓ SOL&PFR conditions

• Radial decay length for temperature and density.

✓Targets

• Sheath boundary, sheath heat transmission coefficients γ_e=4.5, γ_i=2.5, recycling coefficients=1.0.

• C from physical sputtering (Roth-Bodansky formula) and chemical sputtering yield 0.02 for all divertor targets.

✓ Others

• No drifts for computational convergence easily;

• All the gas impurities (N, Ne, Ar) are considered atom.

3. A+M data application in SOLPS

3.1. Atomic reaction rate coefficients involved in B2.5

➢ **Atomic reaction rate coefficients needed in B2.5 are from database**

• STRAHL-a collisional-radiative package developed at IPP-Garching;

• ADAS-(Atomic Data and Analysis Structure) a complete collisional-radiative atomic physics database, actively being maintained and upgraded.

➢ **Uncertainties in atomic data and surface data**

• Some different exists between ADAS and STRAHL, especially for CX (see Fig.2 for an example), ADAS is recommended and the Accuracy of ADAS is ~10%-20%.

• High accuracy data CX reactions for impurity is lack, especially for highly ionized state of high-z elements in low energy region (Te<10eV)!!!

• Physical and chemical sputtering is very important for impurities sources, however, chemical sputtering yield assume to be a constant in SOLPS.

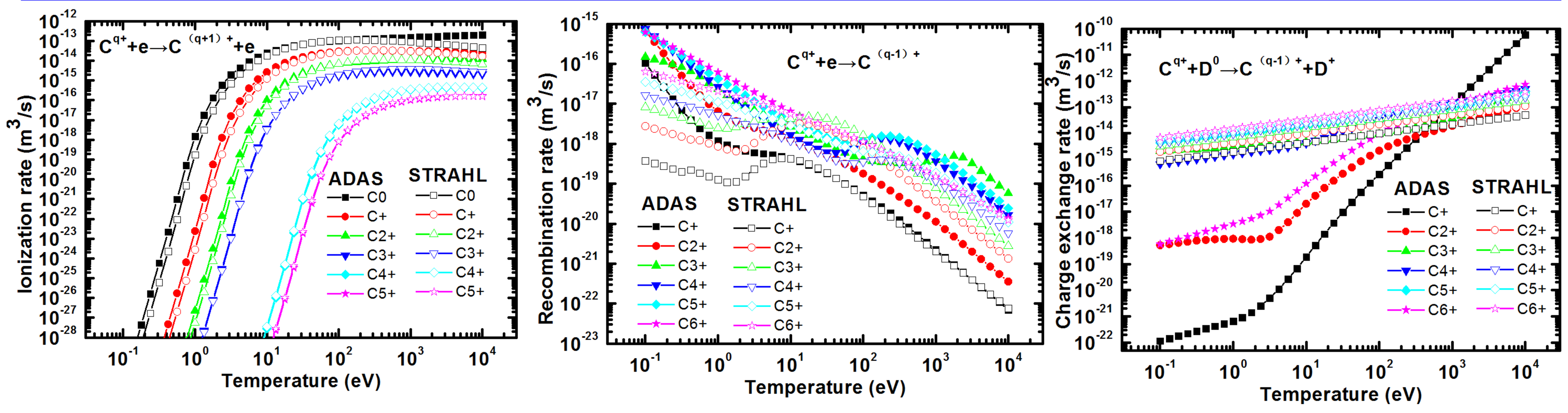

Fig.2. Ionization, recombination and charge exchange of C^{q+} as a function of temperature for a fixed density (n_e=1.0×$10^{19}m^{-3}$) .

3.2. A+M data involved in EIRENE

Table 1. Deuterium neutral reactions included in Eirene

Species	Index	Reaction	Type
Atom	1	$D+e \to D^++2e$	Ionization
	2	$D+D^+ \to D+D^+$	Elastic collision
	3	$D+D^+ \to D^++D$	Charge exchange
Molecule	4	$D_2+e \to D_2^++2e$	Ionization
	5	$D_2+e \to D+D+e$	Dissociation
	6	$D_2+e \to D+D^+ +e$	Ionizing dissociation
	7	$D^++D_2 \to D^+ + D_2$	Elastic collision
	8	$D^+ + D_2 \to D+ D_2^+$	Charge exchange
Molecular ion	9	$D_2^++e \to D+D^+ +e$	Dissociation
	10	$D_2^++e \to D^++D^+$	Ionizing dissociation
	11	$D_2^++e \to D+D$	Recombination
Ion	12	$D^+ +e \to D+h\nu$	Recombination

➢ **Three volumetric processes for molecues involving** —— which can be important in the temperature Te ~2eV, especially at the onset of detachment.

Type	Type	Reaction	Reaction
Molecular assisted recombination	MAR	$D_2+D^+ \to D_2^++D$	$D_2^++e \to D+D$
Molecular assisted dissociation	MAD	$D_2+D^+ \to D_2^++D$	$D_2^++e \to D+D^+ +e$
Molecular assisted ionization	MAI	$D_2+D^+ \to D_2^++D$	$D_2^++e \to D^++D^+$

Table 2. Impurities neutral reactions included in Eirene

Species	Index	Reaction	Type
X(C, N, Ne, Ar)	1	$X + e \to X^++2e$	Ionization
	2	$X^+ +e \to X+ h\nu$	Recombination
	3	$X + D^+ \to X^++D$	Charge exchange

4. Simulation results and comparisons

4.1. Radiated power distribution

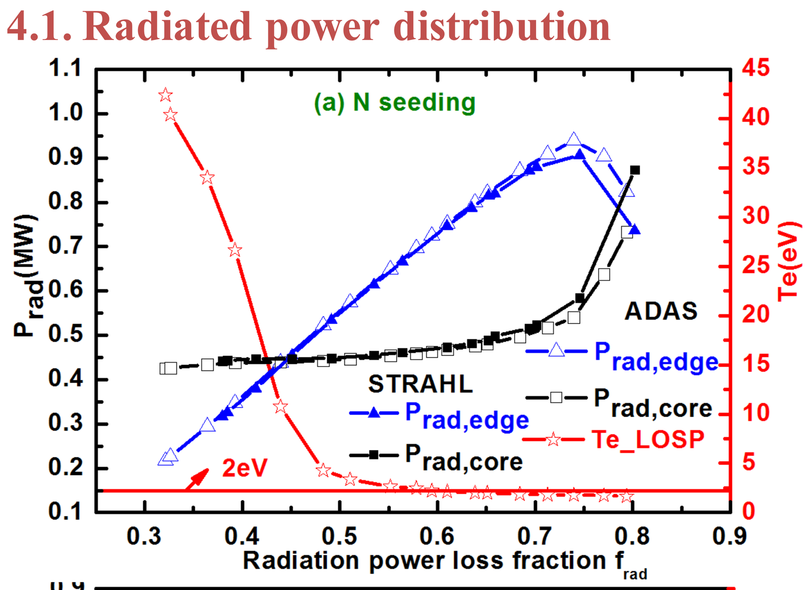

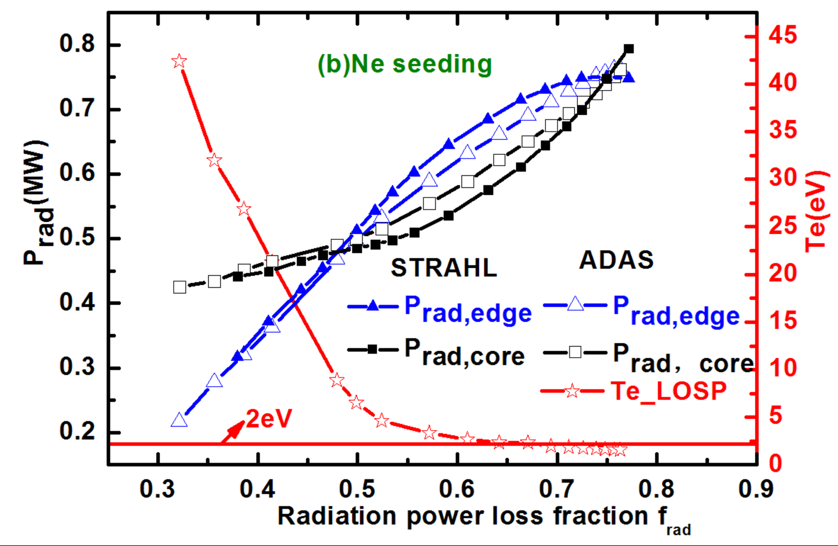

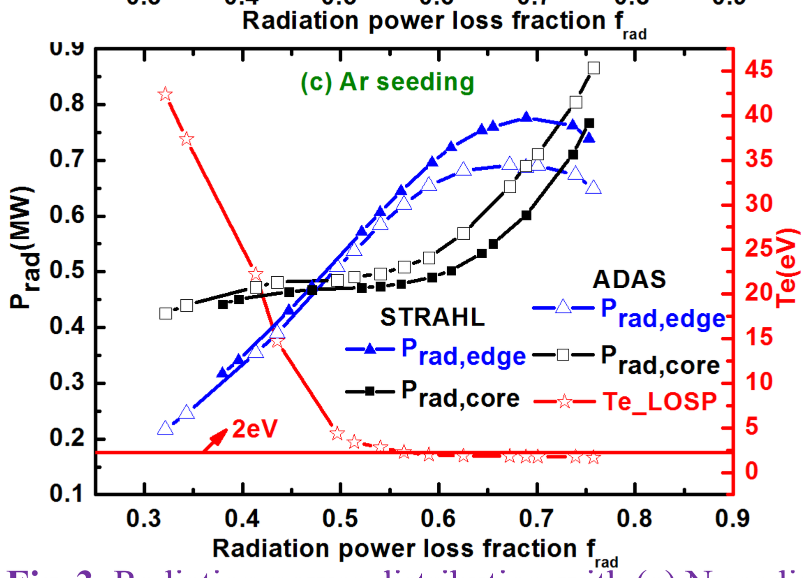

Fig. 3. Radiation power distribution with (a) N seeding , (b) Ne seeding and (c) Ar seeding based on ADAS and STRAHL database.

• $P_{edge, rad}$ =SOL +divertor, outside the sep;

• $P_{core, rad}$ =0.4MW+ $P_{core, SOLPS}$, inside the sep;

• T_{e_LOSP} is the peak temperature at lower outer strike point.

• Radiation power loss fraction f_{rad} = ($P_{rad, SOLPS}$+ 0.4MW)/2MW, 0.4MW = core radiation not accounted in the simulations, which may underestimate $P_{core, rad}$, especially for Ar at high f_{rad};

➢ Max f_{rad} reached ~85% for N seeding, ~75% for Ne and Ar seeding.

➢ N seeding increases the edge radiation power mainly, while Ne and Ar seeding increase the radiation power in both edge and core region.

➢ The divertor get detachment (~2eV) when the impurities puffing rate reach a high level.

➢ The difference between using ADAS and STRAHL database get more significant at high f_{rad} for high-Z impurities Ne and Ar which means there exists a larger uncertainty for high-Z impurity atoms.

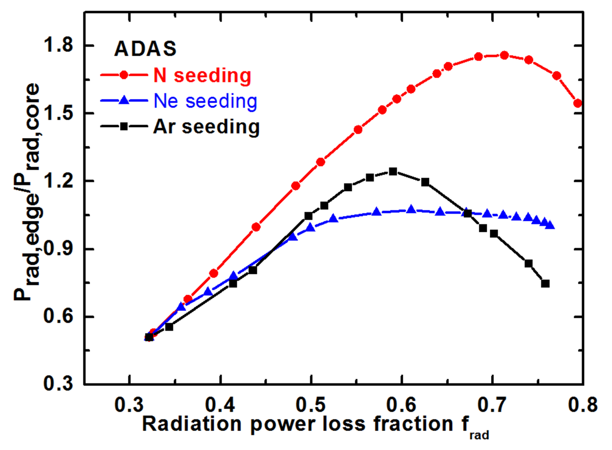

Fig. 4. The ratio of radiation power in edge to core region with N, Ne and Ar seeding.

4.2. P_{sep} and Z_{eff}

➢ Power across separatrix P_{sep} and edge Z_{eff} are proved to has a strong relation with core confinement factor H_{98}.

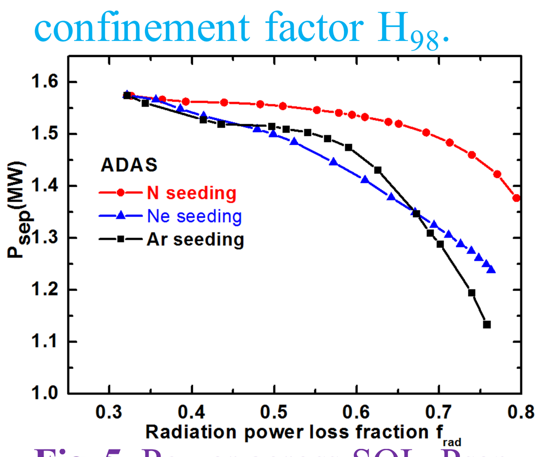

Fig. 5. Power across SOL Psep against f_{rad} with N, Ne and Ar seeding.

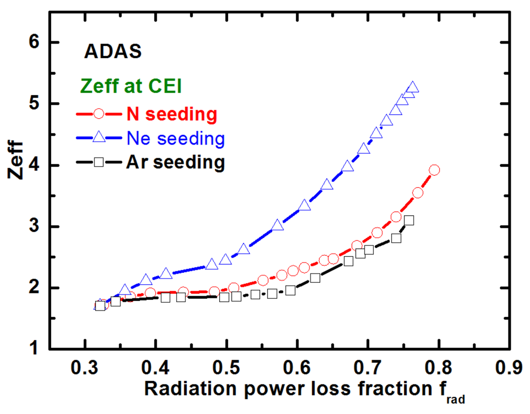

Fig. 6. Effective charge Z_{eff} against f_{rad} with N, Ne and Ar seeding.

➢ The radiation power ratio of edge to core for N, Ne and Ar seeding case are all increases as f_{rad} and reach the max value, then drop which mean the radiation region move into the separatrix gradually.

➢ P_{sep} decreases faster for Ne and Ar seeding than.

➢ N has a larger edge Z_{eff} than Ne and Ar, Ne is more easier to access into sep than N and Ar due to its longer ionization free path , the divertor screening from impurities get weaker at a high level f_{rad}.

4.3. Radiative power loss rate

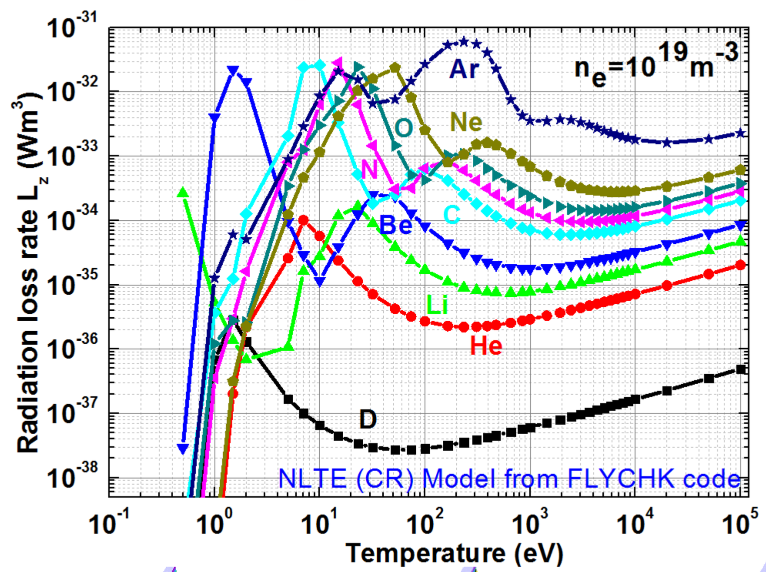

Fig. 7. Radiative power loss rates of some Important elements in tokamak plasma.

Impurity	Radiation Te	Radiation region
N	10-30eV	Divertor
Ne	30-80eV	Divertor
Ar	10-30, 100-500eV	Divertor, pedestal or core

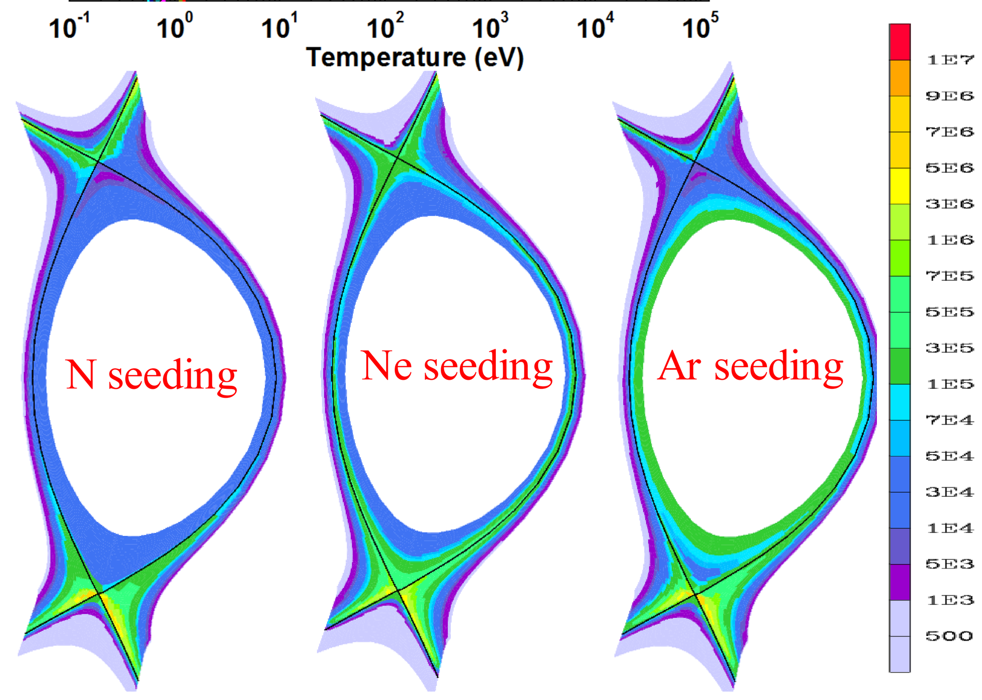

➢ Both N and Ar has strong radiated power in diverot region, while Ar Radiation inside separatrix also significant.

➢ Ne mainly radiated power around X-point and separatrix.

Fig. 8. Total line radiation rate (w/m³) for N^0-N^{7+}, Ne^0-Ne^{10+} and Ar^0-Ar^{18+} in N and Ar seeding plasma at f_{rad}~65%.

5. Conclusion

➢ Radiation divertor with N, Ne and Ar impurities seeding on EAST has been simulated by using SOLPS5.0 code based on ADAS and STRAHL database.

➢ N, Ne and Ar seeding can reduce Te peak and heat flux load at divertor targets similarly.

➢ The power across separatrix decrease faster for Ne and Ar seeding than N which means relative high-Z impurities will reduce the core power significantly which may degrade the core performance when the heating power is not high like EAST.

➢ The radiative loss rate of different impurities show that Ar is a good radiator for divertor and core region, it may be suitable for ITER or DEMO to reduce the power enter into SOL region.

➢ High accuracy A+M data for impurities, especially for high-Z impurities are really necessary for the modeling code to predict burning plasma devices, such as ITER, CFETR and DEMO.

6. Acknowledgements

We would like to express our gratitude to D. P. Coster for the help in application of SOLPS code. This work is supported by National Magnetic Confinement Fusion Science Program of China under contract nos. 2014GB106005 and 2015GB101000, National Nature Science Foundation of China under contract nos. 11305206, 11275231, 11405213and 11575244.